Initial-state-selected MNN Auger spectroscopy of atomic rubidium

J. Keskinen,[1,*] P. Lablanquie,[2] F. Penent,[2] J. Palaudoux,[2] L. Andric,[2,3] D. Cubaynes,[4] J.-M. Bizau,[4] M. Huttula,[1] and K. Jänkälä[1]

[1]*Nano and Molecular Systems Research Unit, University of Oulu, P.O. Box 3000, 90014 Oulu, Finland*

[2]*Sorbonne Universités, UPMC Université Paris 06, CNRS, UMR 7614, Laboratoire de Chimie Physique-Matiére et Rayonnement, 4 place Jussieu, F-75252 Paris Cedex 05, France*

[3]*Université Paris-Est, 5 boulevard Descartes, F-77454 Marne-la Vallée Cedex 2, France*

[4]*Institut des Sciences Moléculaires d'Orsay (ISMO), CNRS, Université Paris Paris-Sud, Université Paris-Saclay, F-91405 Orsay, France*

(Received 10 February 2017; published 5 April 2017)

The $M_{4,5}N_{2,3}N_{2,3}$ and $M_{4,5}N_1N_{2,3}$ Auger decay of atomic Rb have been studied by using photoelectron-Auger electron coincidence measurements that enable initial ionic state selected Auger spectroscopy. The Auger spectra in the present study are separated by the total angular momentum j of the $3d$ hole and the orbital of the valence electron $n\ell$ after photoionization. It is shown that the technique allows isolating overlapping features and the study of otherwise unobservable spectral details, from which the presence of shake-down transitions during normal Auger decay is demonstrated experimentally. The technique allows also probing the effects of initial state parity and electron correlation in Auger electron spectroscopy. The observed spectral features are interpreted with theoretical predictions obtained from configuration interaction Dirac-Fock approach.

DOI: 10.1103/PhysRevA.95.043402

I. INTRODUCTION

Rubidium is an alkali metal atom with electronic configuration [Ar] $3d^{10}4s^24p^65s$ in its ground state. During an ionization process the valence $5s$ electron may undergo a shake-up transition into an energetically higher Rydberg orbital creating a so-called satellite spectrum with higher binding energy than the direct process. Since the $5s$ orbital of Rb is above a closed-shell inner-valence orbital structure, the shake-up probability is considerably high. For example, intensity of the satellite spectrum is about 20% of the total photoionization cross section at high energy $3d$ photoionization [1]. However, due to weak Coulomb interaction between the valence electron and the hole created by a core-ionization process, the satellite spectrum of Rb is remarkably clear and straightforward to interpret. In the present study we have used this to our advantage to probe the effects of the valence electron orbital to the MNN Auger decay of Rb.

Study of Auger decay of excited atoms is a difficult task. On one hand, problems arise from preparing atoms into specific excited states and, on the other, a general tendency of Auger spectra appearing at the same kinetic energy region, despite their initial state. The latter causes the measured spectrum to be composed of an incoherent sum of overlapping Auger spectra from multiple initial ionic states, possibly smearing out the fine details. Auger spectra of $ns \rightarrow n'\ell$ excited alkali atoms have been measured using laser excitation prior to ionization [1–5]. The method is selective, but limited to small excitation energies and dipole allowed transitions. It also does not provide precise initial state selection for Auger transitions. In this study we utilize a shake-up process to generate excited ionic states and an electron-electron coincidence technique to segregate the Auger spectra resulting from the different initial states.

The nature of the multielectron coincidence spectroscopy measurements makes it possible to select individual electronic states and the decay paths these states follow. Photoelectron-Auger electron coincidences have been used for separating Auger spectra from different ionic states, for example in Ar [6], Xe [7], Kr [8], and Hg [9], but to our knowledge it has not been utilized in the study of Auger decay of photoionization satellite states thus far. In the present case of Rb $3d$ photoionization we have selected various $3d_j^{-1}n\ell$ ionic states by recording the photoelectron arising from the creation of the state in coincidence with the subsequent Auger electron leading to $4s4p^5n'\ell'$ and $4s^24p^4n'\ell'$ final doubly ionized configurations. The initial states of the recorded Auger spectra are thus separated by the total angular momentum j of the $3d_j$ hole, and principal quantum number n and orbital angular momentum ℓ of the valence electron. This enables us to probe the effects of changing the aforementioned properties to the MNN Auger decay of rubidium.

In addition, due to considerable reduction of overlapping features in the initial-state-selected Auger spectra, we are able to distinguish shake-down processes associated with the $M_{4,5}N_{2,3}N_{2,3}$ decay of initially $3d_j^{-1}(5s \rightarrow n'\ell')$ excited states. Observation of shake-down lines in photoionization [10–13] and *resonant* Auger decay [14,15] have been reported in the past, but to the best of our knowledge, this is the first time when shake-down lines are unambiguously identified in *normal* Auger decay process.

II. EXPERIMENT

The measurements were carried out at the PLÉIADES beamline of the SOLEIL synchrotron in Saint-Aubin, France [16]. A 2-m-long time-of-flight type magnetic bottle setup HERMES (High Energy Resolution Multi Electron Spectrometer) [8] was used to collect the electrons emitted from the sample. The spectrometer is based on the use of two magnetic field regions. The first one is created by a strong SmCo permanent magnet close to the interaction region that acts as a magnetic mirror deflecting the electrons towards the flight tube. The second is a weak field solenoid magnet that is directed parallel to the flight tube, providing a guiding field for the electrons along the tube. The electrons were detected

*Corresponding author: juho.keskinen@oulu.fi

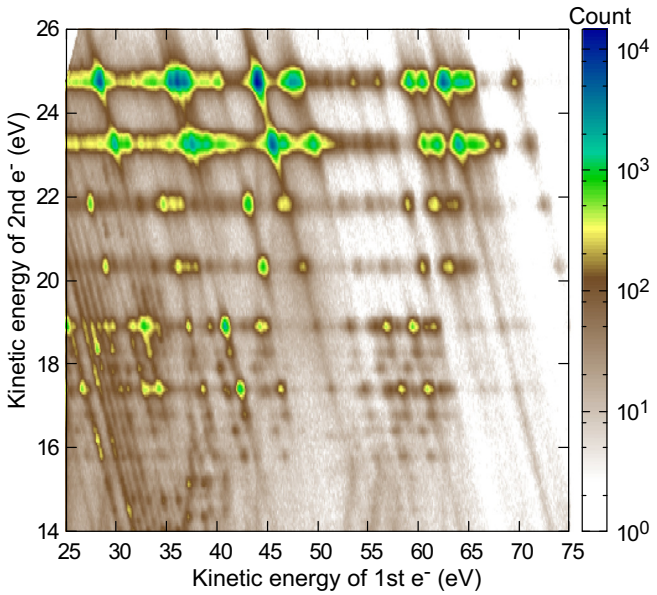

FIG. 1. Two-dimensional correlation map of electrons detected in coincidence following $3d$ photoionization and Auger decay of atomic Rb at the photon energy of 142 eV. Electron counts represented by colors are given in logarithmic scale.

using microchannel plates and the flight times were measured by a time-to-digital converter having a 120 ps discretization step. The energy resolution $\Delta E/E$ of the spectrometer was estimated to be about 1.6% for kinetic energies above 1 eV.

The photon energy used to ionize the target was kept at $h\nu = 142$ eV, which places the $3d$ photoelectron spectrum just below the $M_{4,5}N_1N_{2,3}$ Auger spectrum in kinetic energy [17]. The synchrotron was run in single-bunch mode in order to acquire the time structure (one bunch in every 1184 ns) needed for time-of-flight type of measurements. The sample vapor was produced in a resistively heated oven at the temperature of 155 °C.

Figure 1 shows an example of raw electron-electron coincidence data from the measurements. The data are presented as a coincidence map, in which the horizontal axis corresponds to the kinetic energy of the first electron and the vertical axis gives the energy of the second electron detected in coincidence with the faster one. The number of electrons detected in each point of the map is represented by color. As the photon energy was chosen so that the $3d$ photolines appear below the Auger electron spectrum in kinetic energy, the photoelectrons create horizontal lines. Along the x axis within these lines one can locate the MNN Auger final states as intense spots. The spots are elongated to diagonal lines due to energy conservation present in $h\nu + A \rightarrow A^{++} + e_p + e_A$ scattering process, where normal Auger decay can be considered as resonance in double ionization continuum.

By taking a projection of the map in Fig. 1 onto the vertical axis one can obtain a traditional noncoincident photoelectron spectrum and projection along the horizontal axis gives the Auger spectrum. By taking into account only the counts within selected horizontal slices, it is possible to isolate some of the initial states of the total Auger spectrum. The final spectra were constructed from such slices by binning along the total excess energy (i.e., integrating along diagonal), and recalibrating the spectra back to the kinetic energy scale of the Auger electrons. The procedure improves resolution by removing the broadening caused by post-collision interaction.

III. CALCULATIONS

The atomic state calculations were performed using atomic structure code GRASP2K [18,19] that uses the relativistic multiconfiguration Dirac-Fock (MCDF) approach. Within the MCDF method one is able to obtain the final atomic state functions (ASF) by diagonalizing the Hamiltonian matrix in the basis of jj-coupled antisymmetric configuration state functions (CSF) of the same total angular momentum and parity. The method uses a Dirac-Coulomb Hamiltonian which makes it inherently relativistic. During the calculations an average level scheme was used to obtain the radial wave functions meaning that the code was used to optimize the orbitals by minimizing the average energy of the CSFs. The ASF mixing coefficients and state energies were then computed using the RELCI component of the RATIP package [20,21].

Relative photoionization intensities for overlapping lines were calculated by assuming statistical weights given by the $2J + 1$ degeneracy of ASF states $|PJM\rangle$. The Auger decay was treated as a two-step process, in which the first step consists of photoionization of the target and the second step emission of an Auger electron. The number of emitted Auger electrons to a particular doubly ionized final state is thus proportional to the product of the photoionization cross section and the Auger decay rate, divided by the total decay rate of the intermediate singly ionized state [22]. Calculation of Auger decay matrix elements was performed with the AUGER component of the RATIP suite [20,21].

In the case of both $M_{4,5}N_{2,3}N_{2,3}$ and $M_{4,5}N_1N_{2,3}$ transitions, a separate simulation was run for each of the studied valence states ($5s$, $5p$, $5d$, $6s$, $6p$, and $7s$). The initial state in each case consists of the nonrelativistic configuration $3d^{10}4s^24p^6n\ell$. The intermediate $3d$ hole states are

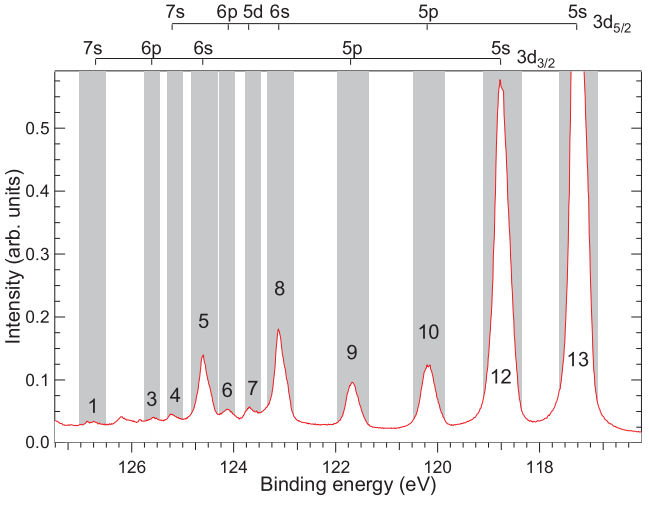

FIG. 2. Rb $3d$ photoelectron spectrum measured at the photon energy of $h\nu = 142$ eV. Gray columns represent the limits used for the selection of the initial ionic states. Numbering of the peaks follows Ref. [1].

described by a set of nonrelativistic configurations, which are for the $5s/d$ states $3d^9 4s^2 4p^6[5s, 4d, 5d, 6d]$, for the $5p$ state $3d^9 4s^2 4p^6[5p, 6p]$ (only $3d^9 4s^2 4p^6 5p$ in the case of $M_{4,5}N_1N_{2,3}$), for the $6s$ state $3d^9 4s^2 4p^6[6s, 5d, 7s]$, for the $6p$ state $3d^9 4s^2 4p^6[6p, 7p]$ (only $3d^9 4s^2 4p^6 6p$ in the case of $M_{4,5}N_1N_{2,3}$), and for the $7s$ state $3d^9 4s^2 4p^6 7s$. The final states of the studied transitions consist of configurations $3d^{10}[4s^2 4p^4, 4s4p^5, 4p^6]n\ell$ and $3d^{10}[4s^2 4p^5, 4s4p^6]$ in the case of $M_{4,5}N_{2,3}N_{2,3}$ and of $3d^{10}4s^2 4p^5$, $3d^{10}4s4p^5 n\ell$, and $3d^{10}4s^2 4p^3[n\ell^2, n'\ell'^2, n\ell\, n'\ell']$ (excluding the $4d5d$ combination for computational reasons) in the case of $M_{4,5}N_1N_{2,3}$. In the aforementioned configurations n and ℓ denote, respectively, the main quantum number and orbital angular momentum of the particular simulated valence state, whereas n' and ℓ' go through those of the other valence states which were included in the same run.

IV. DISCUSSION

Figure 2 represents the photoelectron spectrum resulting from the $3d$ ionization of atomic Rb. The spectrum has been extracted from the electron-electron coincidence data, of which an example is presented in Fig. 1 by projecting the data onto the kinetic energy axis of the photoelectron using a fixed binning value of 0.01 eV. The resulting spectrum was fitted with peaks defined by the Voigt line shape. Energy differences between the peaks were obtained from Ref. [1]. The fitted spectrum was used to determine limits for initial state selection of the Auger decay. The limits are presented as gray columns in Fig. 2.

A. Auger decay of excited states

The population distribution graphs of the final states of the initial ionic state selected $M_{4,5}N_{2,3}N_{2,3}$ and $M_{4,5}N_1N_{2,3}$ Auger decays are presented in Figs. 3 and 4, respectively. The left-hand side columns give the spectra extracted from the collected data and the right-hand side columns the corresponding theoretical simulations. Labeling of the initial states follows the labeling in Fig. 2. Figures 3(a) and 3(b) and Figs. 4(a) and 4(b) are separated by the angular momentum j of the $3d$ hole, and the different horizontal panels in the

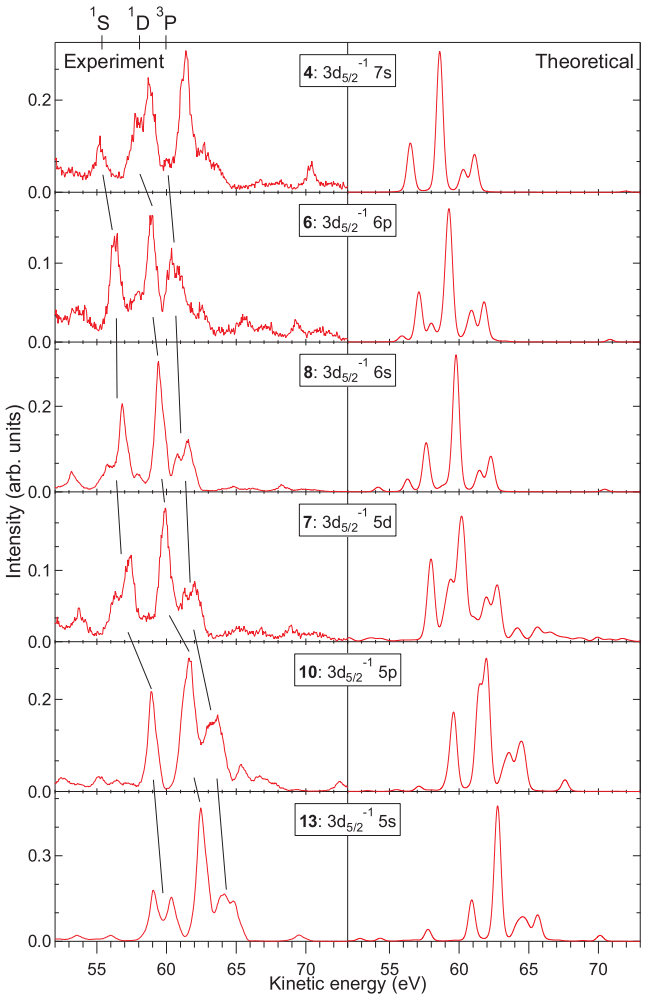

(a) Auger decay of Rb $3d_{5/2}^{-1}nl$ configurations.

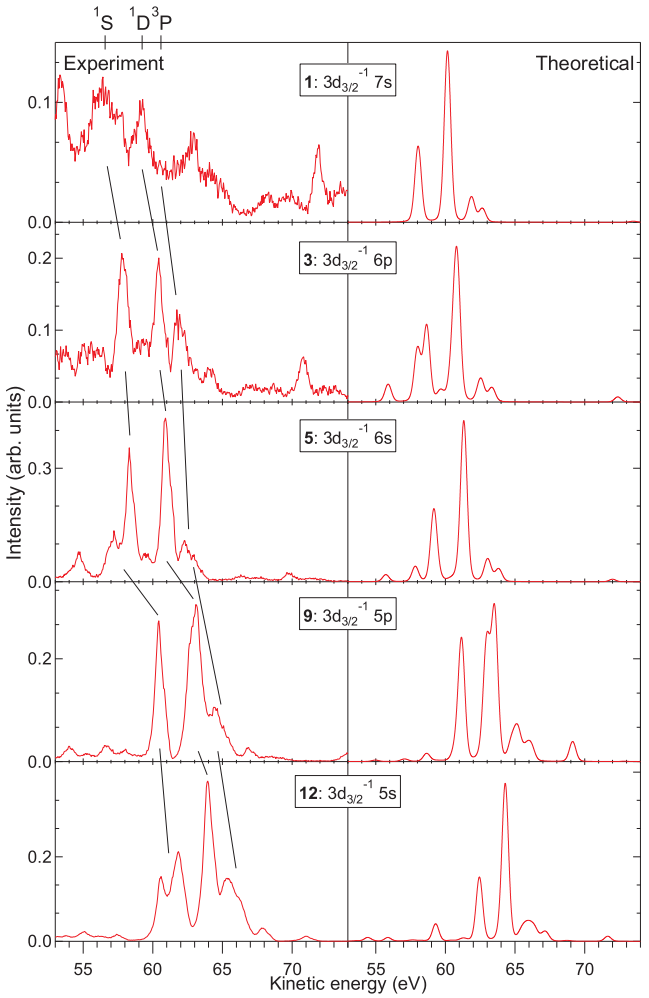

(b) Auger decay of Rb $3d_{3/2}^{-1}nl$ configurations.

FIG. 3. (a) Auger decay of Rb $3d_{5/2}^{-1}nl$ configurations with initial ionic state selected $M_5N_{2,3}N_{2,3}$. (b) Auger decay of Rb $3d_{3/2}^{-1}nl$ configurations with initial ionic state selected $M_4N_{2,3}N_{2,3}$. Left columns show the experiment and the right columns the corresponding simulations. Labels in the middle specify the initial ionic configuration.

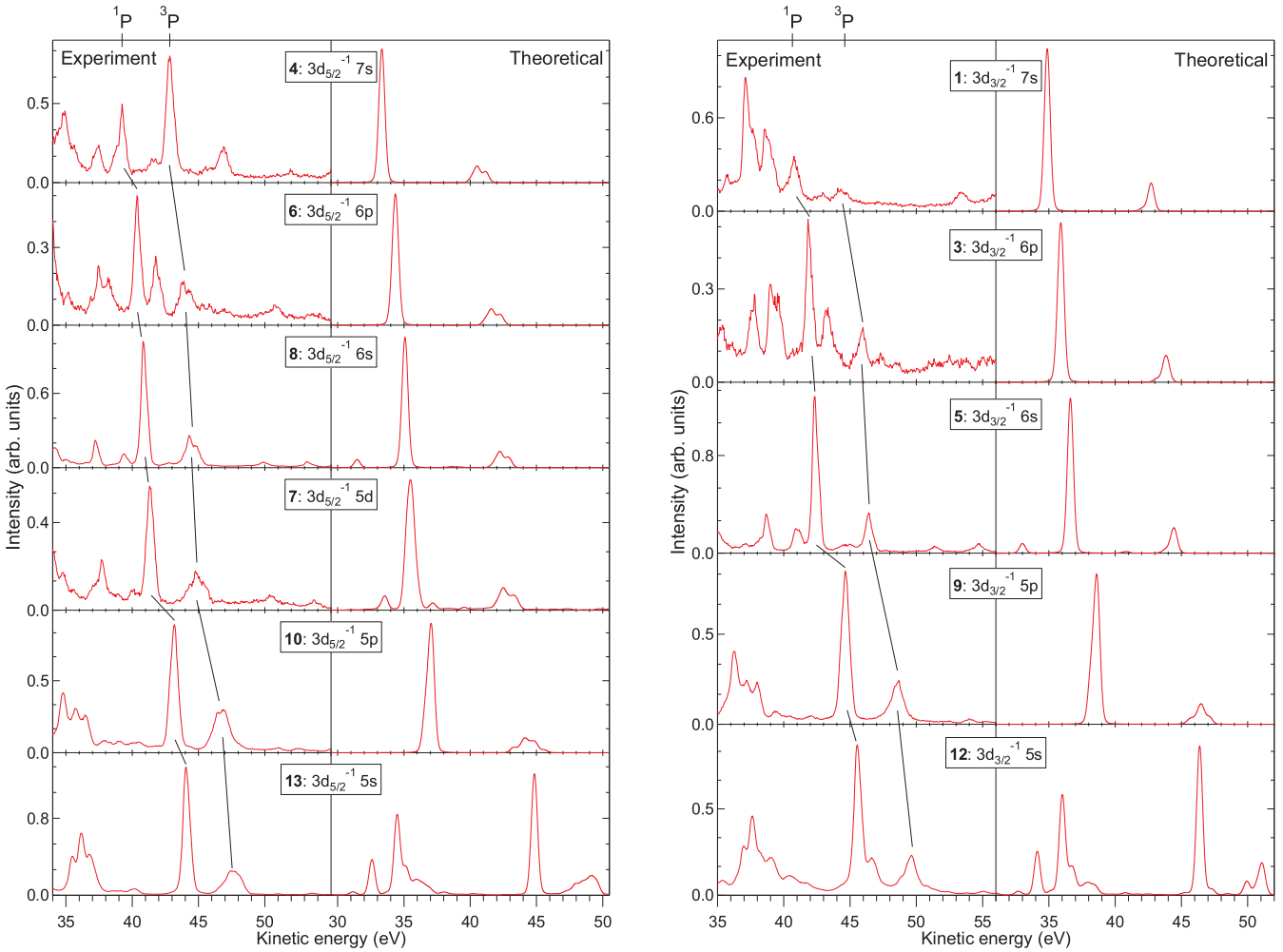

(a) Auger decay of Rb $3d_{5/2}^{-1}nl$ configurations.

(b) Auger decay of Rb $3d_{3/2}^{-1}nl$ configurations.

FIG. 4. (a) Auger decay of Rb $3d_{5/2}^{-1}nl$ configurations with initial ionic state selected $M_5N_1N_{2,3}$. (b) Auger decay of Rb $3d_{3/2}^{-1}nl$ configurations with initial ionic state selected $M_4N_1N_{2,3}$. Left columns show the experiment and the right columns the corresponding simulations. Labels in the middle specify the initial ionic configuration.

figures are identified by the orbital $n\ell$ of the outermost valence electron, with the exception of the highest excited states where the configurations are not completely unique due to small energy differences of the initial states. In Figs. 3(b) and 4(b) initial configuration $3d_{3/2}^{-1}5d$ is not shown because it overlaps almost completely with the $3d_{5/2}^{-1}7s$ configuration [1]. The contribution from $3d_{3/2}^{-1}5d$ is therefore present in the panel showing the $3d_{5/2}^{-1}7s$ spectrum. For example, the highest peak at around 62.5 eV in the $3d_{5/2}^{-1}7s$ panel of Fig. 3(a) originates from $3d_{3/2}^{-1}5d$. It is emphasized that since the splitting arising from the Coulomb interaction between the $3d$ hole and the $n\ell$ valence electron is considerably smaller (in the range of few meV) than the lifetime broadening, the spectra are not strictly initial-state-selected regarding the total angular momentum J of individual states. This has been taken into account in the theoretical simulations.

In the case of $M_{4,5}N_{2,3}N_{2,3}$ Auger spectra shown in Fig. 3, the extracted graphs are characterized by groups of peaks identifiable as $4p^{-2}(^3P)n\ell$, $4p^{-2}(^1D)n\ell$, and $4p^{-2}(^1S)n\ell$ in the order of descending kinetic energy starting at around 65 eV in the case of $5s$. As can be seen, except for a constant shift in kinetic energy, the orbital of the outermost electron does not cause large changes to the overall shape of the Auger spectra. Few subtle differences can however be observed. Most notably, in the comparison of $3d^{-1}5p$ and $3d^{-1}6p$ spectra to the $3d^{-1}5s$, $3d^{-1}5d$, and $3d^{-1}6s$ spectra, the ns and nd cases exhibit an additional peak on the lower kinetic energy side of the $4p^{-2}(^1S)n\ell$ feature. According to our calculations this peak arises from the ns orbitals of the final state mixing with the $5d$ orbital. As the correlation with the ns valence electron with $5d$ decreases as a function of increasing n, the intensity of the peak lowers so that it practically disappears in the case of $7s$, where it is expected to appear at the kinetic energy region below 55 eV. Because $4p^{-2}np$ configurations have different parity than $4p^{-2}nd$, np cases do not mix with nd configurations via single electron excitation. Therefore the additional peak is completely absent in the Auger decay spectra to $4p^{-2}np$ final states. One can also see that if the orbital angular momentum ℓ is larger than 0, the $4p^{-2}(^3P)n\ell$ feature (the highest peak) as shown in Fig. 3 is broader than in ns cases. The reason is that the peak is in fact split into two lines separated by spin-orbit splitting of the valence electron.

The splitting is missing in the ns cases and is the largest for the $5d$ case. In addition we can observe small features at higher kinetic energies above the main spectrum in all spectra, except in the $5s$ case. These features are caused by shake-down Auger transitions, as discussed in the next section.

The lines caused by the $M_{4,5}N_1N_{2,3}$ Auger decay seen in the panels of Fig. 4 feature an intense peak identifiable as $4s^{-1}4p^{-1}(^1P)n\ell$ in the 40–45 eV kinetic energy range and a wider structure $4s^{-1}4p^{-1}(^3P)n\ell$ on its higher energy side. The structure just above the 35 eV mark in the case of $5s$ arises from the mixing of states from $4s^{-1}4p^{-1}5s$ configuration with $4s^24p^{-3}5s4d$ and $4s^24p^{-3}4d6s$ configurations. The most comprehensive theoretical simulation, run only for the $4s^{-1}4p^{-1}5s$ case, including contributions from $4s^{-1}4p^{-1}[4d,5d,6s]$ was the only one able to reproduce the structure. Inclusion of these correlating configurations shifted also the spectrum about 6 eV towards higher kinetic energy, giving a good agreement with the experiment. The simulations of the higher excited valence initial states were, for computational reasons, less comprehensive and therefore do not reproduce the aforementioned structure and the predicted kinetic energies are about 6 eV too low. Unlike with $M_{4,5}N_{2,3}N_{2,3}$ there is no large differences in the number of lines between the decays of even and odd parity initial states.

B. Shake-down transitions

From Fig. 3, in all cases except $5s$, one can observe spectral features at about 65–70 eV kinetic energy that are not reproduced by the present calculations. The reason is that the structures can be identified to be caused by monopole and conjugate shake-down transitions during the MNN Auger decay. The process, in the case of spectra shown in Fig. 3, can be written as

$$3d^94s^24p^6n\ell \rightarrow 3d^{10}4s^24p^4n'\ell' + \epsilon_a^-, \qquad (1)$$

where $n\ell$ is a higher Rydberg orbital than $n'\ell'$. Because $5s$ is the lowest Rydberg orbital of Rb, the shake-down process obviously cannot happen in the case when the valence electron was not excited during ionization. Qualitatively the process can be understood so that the energy released by the $n\ell \rightarrow n'\ell'$ shake-down during the Auger process is taken by the emitted Auger electron ϵ_a^-, which appears higher in kinetic energy than the electrons from decays in which shake-down did not occur. Shake-down processes have been observed in photoionization of laser excited atoms (e.g., [10–13]) and resonant Auger decay [14,15], which by nature are more initial state selective and have thus less overlapping spectral features than normal Auger decays. To our knowledge this is the first time shake-down lines associated with normal Auger decay have been identified with certainty.

Existence of the shake-down lines was confirmed and studied by comparing the experimental spectral features of the $M_{4,5}N_{2,3}N_{2,3}(n'\ell' = 5s)$ Auger spectra to the $M_{4,5}N_{2,3}N_{2,3}(n\ell = 5p)$ case, and $M_{4,5}N_{2,3}N_{2,3}(n'\ell' = 5s$ and $5p)$ to the $M_{4,5}N_{2,3}N_{2,3}(n\ell = 6s)$ case. The matching was done by scaling down and shifting the Auger graphs in energy by taking into account the energy released by the $n\ell \rightarrow n'\ell'$ shake-down. The required kinetic energy shift was determined experimentally from the photoelectron spectrum because it has to be the same as the binding energy difference of the corresponding initial states. For example, in the case of $5p \rightarrow 5s$ shake-down we took the Auger spectrum from $3d_j^{-1}5s$ initial state (lowest panel in Fig. 3), shifted it by the binding energy difference of the $3d_j^{-1}5s$ and $3d_j^{-1}5p$ states, laid it over the Auger spectrum from the $3d_j^{-1}5p$ initial state, and scaled down its intensity. The results, which show nearly a perfect visual match, are depicted in Fig. 5.

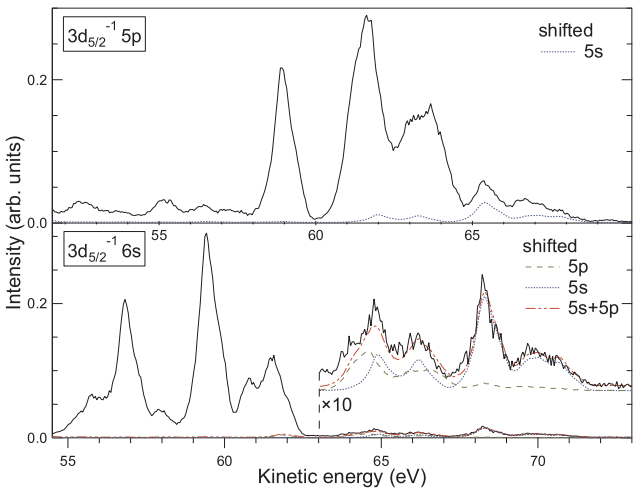

(a) Shake-down following the Rb $3d_{5/2}$ hole state.

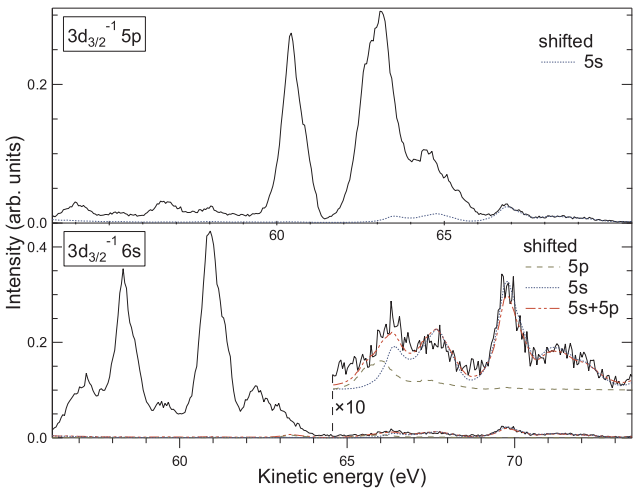

(b) Shake-down following the Rb $3d_{3/2}$ hole state.

FIG. 5. (a) Shake-down following the Rb $3d_{5/2}$ hole state. (b) Shake-down following the Rb $3d_{3/2}$ hole state. Solid line represents the population distribution of final states following the $M_{4,5}N_{2,3}N_{2,3}$ Auger decay of the $5p$ (top) and $6s$ (bottom) valence states of atomic Rb. Dotted and dashed lines represent the distributions for the $5s$ and $5p$ valence states, respectively, but are scaled down in intensity and offset in kinetic energy by the energy differences of the initial states to show the presence of structures caused by $5p \rightarrow 5s$ (top), $6s \rightarrow 5p$ (bottom), and $6s \rightarrow 5s$ (bottom) shake-downs. The line with longer and shorter dashes (bottom) represents the sum of the two shake-downs.

The kinetic energies of the shake-down spectra are precisely correct, but to use the aforementioned process one needs to assume that the overall shape of an Auger spectrum is mainly determined by the final configuration of the decay. In the case of monopole shake-down process, the approximation is expected to hold well because the angular momentum coupling does not differ from the main process. In the case of conjugate shake-down, applicability of the approximation is not obvious, but nevertheless it is seen to work well, at least with the present experimental resolution. The likely reason is that despite the change in orbital angular momentum in the valence, the overall shape of the recorded $M_{4,5}N_{2,3}N_{2,3}(n\ell)$ Auger spectra is dictated by the coupling between the initial $3d^{-1}$ and final $4p^{-2} + \epsilon_a^-$ orbital configurations.

The lines resulting from the aforementioned shake-down processes in Fig. 5 have enough statistics for giving an approximation for the shake-down probabilities. The probabilities were determined by placing the main and energy shifted graphs on top of each other and scaling the intensities until a satisfactory fit was found. Top part of Fig. 5 depicts the contribution of the $5p \rightarrow 5s$ shake-down lines and the bottom part $6s \rightarrow (5p,5s)$ lines. The probabilities of the shake-down processes according to our measurements are [6% for $5p \rightarrow 5s$], [3% for $6s \rightarrow 5s$ $(3d_{5/2})$], [5% for $6s \rightarrow 5s$ $(3d_{3/2})$], and [2% for $6s \rightarrow 5p$]. The probabilities are smaller than for example the corresponding shake-up transitions in $3d$ photoionization [23], but still of considerable magnitude. Note also that interestingly in contrast with the shake-up transitions in photoionization, the probabilities for monopole and conjugate transitions are roughly equal. In the case of analysis of conventional (i.e., not initial-state-selected) Auger spectra, the contribution from shake-down remains small because the probability is multiplied by the probability of shake-up transition during ionization. However, the lines may be observed in high resolution and statistics experiments even without specific state selection.

V. CONCLUSIONS

A photoelectron-Auger electron coincidence study on the synchrotron radiation induced ionization of the $3d$ orbital in atomic rubidium was presented. The resulting electron-electron energy correlation map allowed extraction of initial-state-selected MNN Auger spectra. The spectra enabled the study of the Auger decay as function of the orbital of the valence electron and the total angular momentum of the $3d$ hole. MCDF simulations were used to interpret the observed spectral features.

The study demonstrated that multielectron coincidence measurements can be successfully used for high precision initial ionic state selected Auger spectroscopy of photoionization satellite states, which is very demanding using traditional electron spectroscopy due to severe spectral overlap. The details of the decay provided us the means to observe shake-down transitions during normal Auger decay and to probe the effects the initial ionic state parity and electron correlation have on the final state of the Auger decay.

ACKNOWLEDGMENTS

This work has been financially supported by the Research Council for Natural Sciences and Engineering of the Academy of Finland. J.K. acknowledges EXACTUS-DP (Doctoral Program in Exact Sciences) and the Magnus Ehrnrooth foundation. The experiments were carried out during SOLEIL beamtime project 20131019. The staff of SOLEIL synchrotron and PLÉIADES beamline are acknowledged for assistance during the measurements.

[1] K. Jänkälä, J. Schulz, M. Huttula, A. Caló, S. Urpelainen, S. Heinäsmäki, S. Fritzsche, S. Svensson, S. Aksela, and H. Aksela, Phys. Rev. A **74**, 062704 (2006).

[2] M. Richter, J. M. Bizau, D. Cubaynes, T. Menzel, F. J. Wuilleumier, and B. Carré, Europhys. Lett. **12**, 35 (1990).

[3] K. Jänkälä, R. Sankari, J. Schulz, M. Huttula, A. Caló, S. Heinäsmäki, S. Fritzsche, T. Rander, S. Svensson, S. Aksela, and H. Aksela, Phys. Rev. A **73**, 022720 (2006).

[4] A. Dorn, O. Zatsarinny, and W. Mehlhorn, J. Phys. B **30**, 2975 (1997).

[5] J. Nienhaus, O. I. Zatsarinny, A. Dorn, and W. Mehlhorn, J. Phys. B **30**, 3611 (1997).

[6] P. Lablanquie, L. Andric, J. Palaudoux, U. Becker, M. Braune, J. Viefhaus, J. H. D. Elandc, and F. Penent, J. Electron Spectrosc. Relat. Phenom. **156-158**, 51 (2007).

[7] F. Penent, J. Palaudoux, P. Lablanquie, L. Andric, R. Feifel, and J. H. D. Eland, Phys. Rev. Lett. **95**, 083002 (2005).

[8] J. Palaudoux, P. Lablanquie, L. Andric, K. Ito, E. Shigemasa, J. H. D. Eland, V. Jonauskas, S. Kučas, R. Karazija, and F. Penent, Phys. Rev. A **82**, 043419 (2010).

[9] S.-M. Huttula, J. Soronen, M. Huttula, F. Penent, J. Palaudoux, L. Andric, and P. Lablanquie, J. Phys. B **48**, 115001 (2015).

[10] J. Schulz, M. Tchaplyguine, T. Rander, O. Björneholm, S. Svensson, R. Sankari, S. Heinäsmäki, H. Aksela, S. Aksela, and E. Kukk, Phys. Rev. A **72**, 010702(R) (2005).

[11] J. Schulz, S. Heinäsmäki, R. Sankari, T. Rander, A. Lindblad, H. Bergersen, G. Öhrwall, S. Svensson, E. Kukk, S. Aksela, and H. Aksela, Phys. Rev. A **74**, 012705 (2006).

[12] K. Jänkälä, M. Alagia, V. Feyer, K. C. Prince, and R. Richter, Phys. Rev. A **84**, 053426 (2011).

[13] M. Meyer, A. N. Grum-Grzhimailo, D. Cubaynes, Z. Felfli, E. Heinecke, S. T. Manson, and P. Zimmermann, Phys. Rev. Lett. **107**, 213001 (2011).

[14] S. B. Whitfield, J. Tulkki, and T. Åberg, Phys. Rev. A **44**, R6983(R) (1991).

[15] H. Aksela, M. Kivilompolo, E. Nõmmiste, and S. Aksela, Phys. Rev. Lett. **79**, 4970 (1997).

[16] X.-J. Liu, Q. Miao, F. Gel'mukhanov, M. Patanen, O. Travnikova, C. Nicolas, H. Ågren, K. Ueda, and C. Miron, Nat. Photon. **9**, 120 (2014).

[17] H. Aksela, S. Aksela, R. Lakanen, J. Tulkki, and T. Åberg, Phys. Rev. A **42**, 5193 (1990).
[18] F. A. Parpia, C. Froese Fischer, and I. P. Grant, Comput. Phys. Commun. **94**, 249 (1996).
[19] P. Jönsson, X. He, C. Froese Fischer, and I. P. Grant, Comput. Phys. Commun. **177**, 597 (2007).
[20] S. Fritzsche, J. Electron Spectrosc. Relat. Phenom. **114-116**, 1155 (2001).
[21] S. Fritzsche, Comput. Phys. Commun. **183**, 1525 (2012).
[22] T. Åberg, Phys. Scr. **1992**, 71 (1992).
[23] S. Fritzsche, K. Jänkälä, M. Huttula, S. Urpelainen, and H. Aksela, Phys. Rev. A **78**, 032514 (2008).